

# Structural Characteristics and NO<sub>x</sub> Formation in an Oscillating Stagnation Flat Flame

Yei-Chin Chao, Yau-Wei Huang, and Guan-Ban Chen

Institute of Aeronautics and Astronautics

National Cheng Kung University

Tainan, Taiwan, 701, R.O.C

E-mail: [ycchao@mail.ncku.edu.tw](mailto:ycchao@mail.ncku.edu.tw)

## Extended Abstract

Flame stretch is usually encountered in practical combustion systems. Flame stretch can be induced by aerodynamic straining, flame curvature and flame/flow unsteadiness. Aerodynamic stretch effects are caused by velocity gradients that can strain or contort the reaction zones in combustion environments. The flat flame is an ideal tool for studying aerodynamic stretch because it has well defined velocity gradients and can be numerically modeled by a system of one-dimensional (1-D) equations under suitable assumptions. The flat flame can be established and stabilized in the stagnating flow or counterflow fields. The measurements of global parameters such as flame location and stretch at extinction of flat flames have been studied [1-7]. However, in practical combustion devices the aerodynamic stretch imposed on reaction zones is seldom steady. Many analytical and computational efforts have also been made to investigate the effects of unsteady stretch on flames. [8-13]. Recently, intensive studies on the extinction characteristics in a counterflow flame under periodic stretch or straining due to acoustic excitation have been reported in the literature [10-13]. High frequency excitation is found to sustain higher strain rates and extends the extinction limit. On the other hand, Chen and Driscoll [14] have clearly shown the positive relation of the NO<sub>x</sub> scaling with the global strain rates in jet flames. Further in-depth studies of unsteady NO<sub>x</sub> formation characteristics in combustion systems are of vital importance to the design of the advanced ultra-low NO<sub>x</sub> combustion systems for the next generation, as the flames are strongly influenced by the periodic passing and straining of vortices. However, most NO<sub>x</sub> formation studies are concentrated on steady flames or the mean NO<sub>x</sub> properties.

The oscillating flat flame with prescribed periodic strains rates induced by the oscillating stagnation flowfield of premixed fuel/air jet impinging on an oscillating plate ideally facilitates experimental and computational studies of the effects of unsteady strain rates on the flame structure and combustion characteristics.

The essential features of the current setup and measurement instruments are shown schematically in Fig. 1. The equivalence ratio of the methane-air mixtures is 0.8. The global strain rate,  $a$ , is defined by the ratio of the exit velocity,  $V$ , and the separation distance,  $L$ . The mean separation distance  $L$  between the nozzle and the stagnation plate is adjustable in this study. The instantaneous separation distance =  $L + A \times \sin(\omega t)$ , where  $A$  is the amplitude of the oscillation and  $\omega$  is the angular frequency. A triggering device is designed to trigger the measurement at a prescribed phase relative to the oscillating plate and to align the

measurement data for phase-averaging calculation. The flame images gathered by the CCD camera triggered at different phases are used to identify the flame thickness and location. The shutter time of CCD is 1/500 sec. For temperature measurement, a R-type thermocouple coated with BeO and Y<sub>2</sub>O<sub>3</sub> to eliminate catalytic reaction of platinum in the flame is used. Instantaneous planar NO-LIF images obtained using a tunable KrF excimer laser tuning at 247.9 nm for excitation of the NO A-X(0,2) band, similar to that developed by Schultz et al. [15], are used to detect NO profile for comparison with the numerical results.

In this study, the numerical method is also applied to simulate the flame structure and the combustion characteristics. The numerical simulation is performed with gas-phase only and the surface reaction on the plate is neglected. The governing equations include the Navier-Stokes, energy and mass conservation equations and the species equation. The SPIN code [16] incorporated with the GRI-Mech 2.11 mechanism, which consists of 49 species and 276 elementary steps, is used for numerical simulation and the unsteady term is solved by the second-order implicit scheme.

As shown in Fig. 2a, the white arrowheads indicate the separation distance between the nozzle exit and the plate. Increasing strain rate results in thinner flame and the flame moves toward the plate. The distance  $y$  from the plate to the flame decreases with increasing strain rate in Fig. 2b. However, there is no obvious difference when the normalized distance  $y/L$  from the plane to the flame is compared in the high strain rate region,  $a > 30$ . The flame photographs at different phases, 90°, 0° and 270°, are shown in Fig. 3.

To further look into the structure of the oscillating flat flames, comparison between experimental and computational temperature profiles and the velocity profiles between the nozzle exit and the plate are shown in Fig. 4. The global strain rate at the mean location for three separation distances are  $a = 44.16, 31.17$  and  $24.09 \text{ s}^{-1}$ . The peak flame temperature falls slightly and moves toward the plate as the strain rate is increased due to the thinner flame and less residence time in the reaction zone. As for the velocity profile, a non-reactive flow is characterized by a monotonic transition between the velocities at the boundaries. In the combustion zone, however, there is a profound density change due to the high temperature of the burnt gas. Because of the conservation of the mass flux,  $\rho u$ , there is a deviation from the monotonic behavior in the region of the flame (here in the region 0.6~0.9 cm from the plate in Fig. 4). The slightly lower temperature is obtained from experiment due to the heat transfer to the plate or ambience. However, adiabatic and no-reaction conditions have been assumed on the plate in the simulation.

The mole fraction of the major combustion species is shown in Fig. 5 at various strain rates. The fuel CH<sub>4</sub>, as well as the oxygen O<sub>2</sub>, decreases towards the combustion zone. The minor combustion species such NO<sub>x</sub> and OH are shown in Fig. 6. The OH is usually used to identify the high temperature and combustion zones. From OH profile, it is clear that the combustion zone becomes thinner and closer to the plate when higher strain rate is applied. In Fig. 6, the maximum NO<sub>x</sub> concentrations near the plate decrease with an increase of stretch. This is due to the reduced residence time in high temperature zones. Increasing flame stretch causes decreasing peak temperature and NO production decreases. It is consistent with the results of Ref. [17]. The width of the NO profile becomes narrower with an increase in stretch owing to the increased velocity gradients. It is consistent with the results of Ref. [18]. When unsteady (periodic) strain rate of different amplitudes,  $A = 1, 7 \text{ mm}$  at a frequency of 10 Hz is applied, the structure and combustion species of the oscillating flame show different

characteristics in Fig. 7a. The lowest and highest strain rates occur at  $90^\circ$  and  $270^\circ$ . For the low amplitude case, the OH concentration and  $T_{max}$  peaks in a cycle lag behind the lowest strain rate,  $90^\circ$ , by about 5 ms. This result is similar to the finding of Brown et al. [19]. Around the highest strain rate,  $270^\circ$ , in a cycle, the OH concentration stays low for a long period of time, until near the end of the cycle,  $360^\circ$ . This results in a lower  $T_{max}$  at the end of cycle as compared with that at the beginning of the cycle. This trend of continuous lowering of the  $T_{max}$ , hence weakening the flame, as the oscillation continues will lead to extinction of the flame similar to the results reported in Refs. [6] and [11]. The  $T_{max}$  location is almost stationary, except for very close to  $90^\circ$  and  $270^\circ$ , and  $T_{max}$  stays at the lowest location longer. The NO result reflects the characteristics of OH and  $T_{max}$  mentioned above. In other words, the structural and NO emission characteristics of the flame are relatively insensitive to the variation of the strain rate near the highest strain rate in a cycle. On the other hand, for the high amplitude oscillation case, OH and  $T_{max}$  have an earlier response to the strain rate variation near the lowest strain rate,  $90^\circ$ . However, NO peak still lags by few milliseconds from the lowest strain rate. After the lowest strain rate in a cycle, the “accumulation effect” becomes prevail in the flame, as can be noted from the OH,  $T_{max}$  and NO results in Fig. 7a. When near extinction strain rate, the extinction strain rate of  $2650 \text{ s}^{-1}$  proposed by Stahl et al. [20] and  $1550 \text{ s}^{-1}$  by Law [21], is applied, both the OH,  $T_{max}$  results show that the flame can not survive through the highest strain rate at  $270^\circ$  and extinction occurs before  $270^\circ$  in Fig. 7b. The flame becomes rather insensitive to the variation of the strain rate after the lowest strain rate and stays in high values for OH,  $T_{max}$  and NO throughout the rest of the cycle.

## Reference

1. Tsuji, H., and Yamaoka, I., *Twelfth symposium (International) on Combustion*, The Combustion Institute, Pittsburgh, 1968, pp.997.
2. Ishizuka, S., and Tsuji, H., *Eighteenth symposium (International) on Combustion*, The Combustion Institute, 1981, pp.695.
3. Puri, I.K., and Seshadri K., *Combust. Flame* 65:137-142 (1986).
4. Kee, R.J., Miller, J.A., and Evans, G.H., *Twenty-Second symposium (International) on Combustion*, The Combustion Institute, Pittsburgh, 1988, pp. 1479-1494.
5. Dixon-Lewis, G., and Missaghi, M., *Twenty-Second symposium (International) on Combustion*, The Combustion Institute, Pittsburgh, 1988, pp. 1461-1470.
6. Sung, C.J., and Liu, J.B., and Law, C.K., *Combust. Flame* 106:168-183(1996).
7. Blevins, L.G., and Gore, J.P., *Combust. Flame* 116:546-566 (1999).
8. Clarke, J.F., and Stegen, G.R., *J. Fluid Mech.*, 34, p343 (1968).
9. Haworth, D. C., Drake, M.C., and Blint, R.J., *Combust. Sci. and Tech.* **19**, pp. 287-294(1988).
10. Im, J.S., Law, C.K., Kim, J.S., and Williams, F. A., *Combust. Flame* 100: 21-30 (1995).
11. Sardi, K., Taylor, A.M.K.P., and Whitelaw, J.H., *Combust. Flame* 120: 265-284 (2000).
12. Hirasawa, T., Ueda, T., Matsuo, A., and Mizomoto, M., *Combust. Flame* 121: 312-322 (2000).
13. Im, H.G., Bechtold, J.K., and Law, C.K., *Combust. Flame* 105:358-372 (1996).
14. Chen, R.H., and Driscoll, J.F., *Twenty-Third symposium (International) on Combustion*, The Combustion Institute, Pittsburgh, 1991, pp. 281-288.
15. Schultz, C., Sick, V., Wolfrum, J., Drewws, V., Zahn, M., and Maly, R.m, *Twenty-Sixth symposium (International) on Combustion*, The Combustion Institute, Pittsburgh, 1996, pp. 2597-2604.
16. Coltrin, M.E., Kee, R.J., Evans, G.H., Meeks, E., Rupley, F.M., and Grcar, J.F., Sandia National Laboratories Report SAND91-8003, 1991.
17. Ravikrishna, R. V., Cooper, C. S. and Laurendeau, N. M., *Combust. Flame* 117:810-820 (1999).
18. Im, H.G., Chen, J.H., and Chen, J.Y., *Combust. Flame* 118:204-212 (1999).
19. Brown, T.M., Pitz, R.W., and Sung, C.J., *Twenty-Seventh symposium (International) on*

*Combustion*, The Combustion Institute, Pittsburgh, 1998, pp. 703-710

20. Stahl, G., Rogg, B., and Warnatz, J.: 11<sup>th</sup> ICDERS Conference, Warsaw, Poland (1987).

21. Law, C. K., Zhu, D. L., and Yu, G.: *Twenty-First symposium (International) on Combustion*, The Combustion Institute, Pittsburgh, 1988, pp. 1419-1433

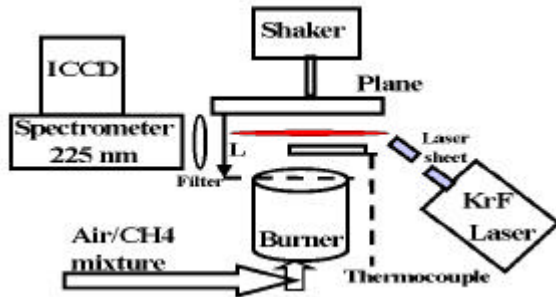


Fig. 1 Schematic diagram of the experimental setup

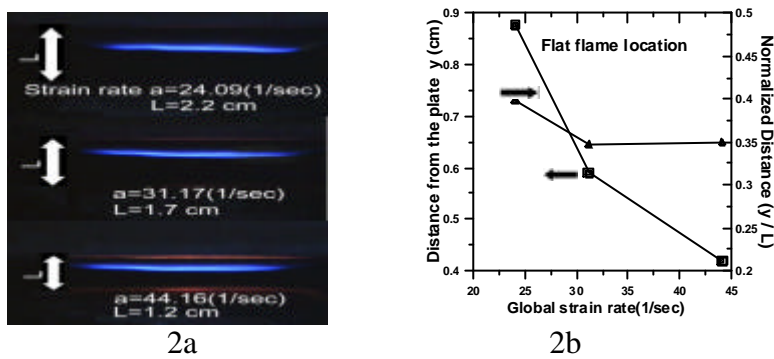


Fig. 2 Flat flame location at various strain rate

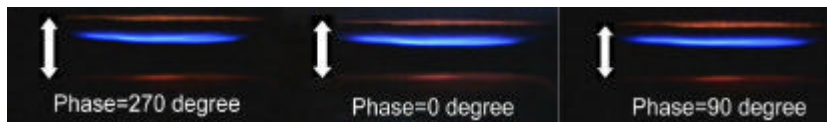


Fig. 3 The flat flame location at various phases

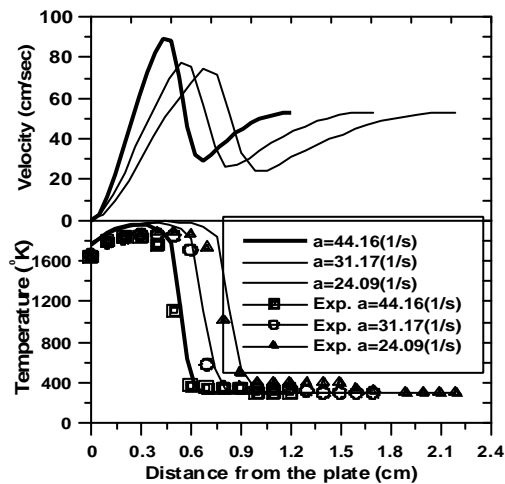


Fig. 4 The velocity and temperature profiles and the comparison between experimental and computed temperature at various strain rates

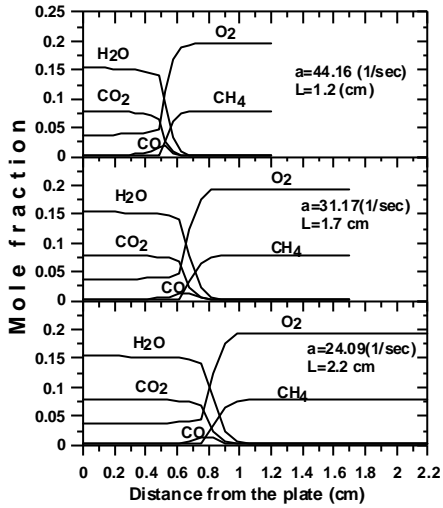


Fig. 5 The major combustion species at various strain rate

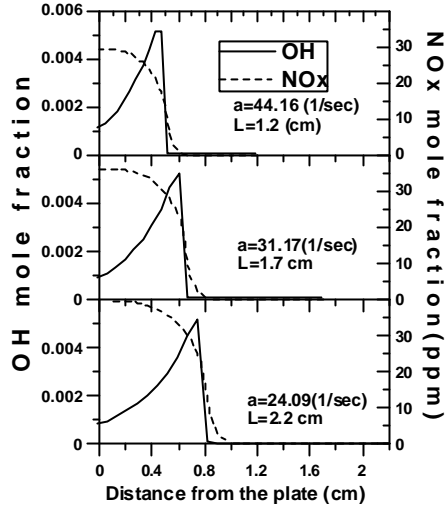


Fig. 6 The minor combustion species at various strain rates

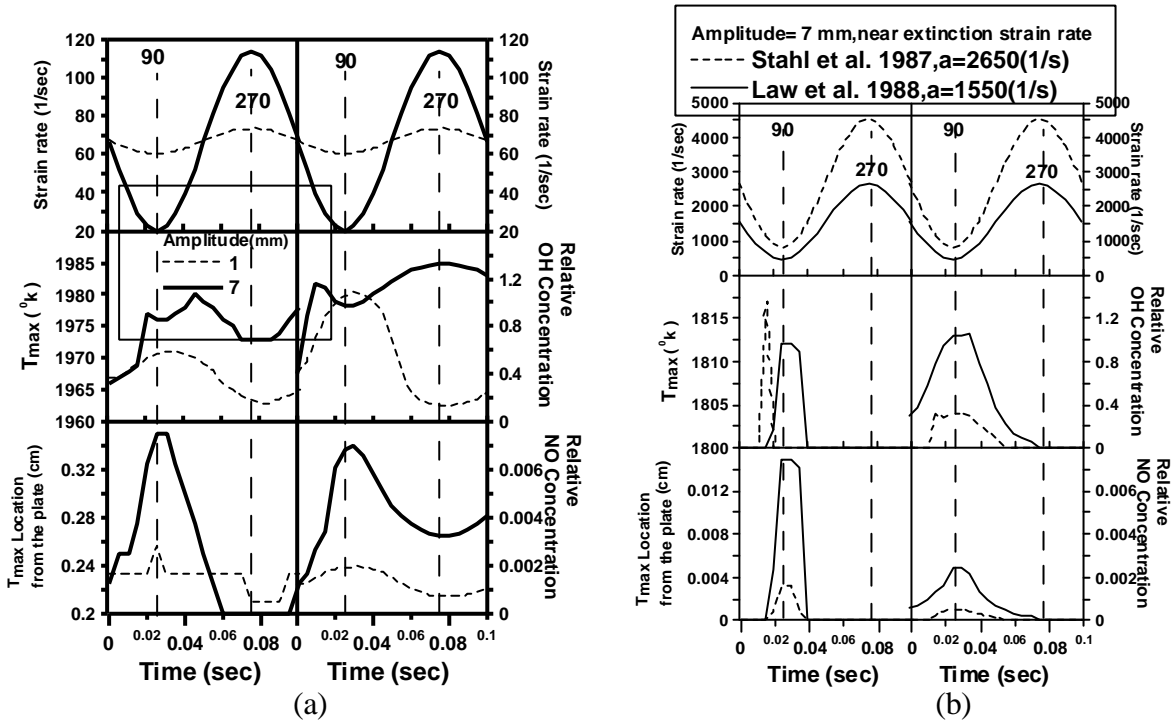


Fig. 7 The structure and combustion species of the oscillating flame at the amplitude  $A=1, 7$  mm and the frequency = 10 Hz (a) far away from the extinction strain rate and (b) near the extinction strain rate.